Optical Engineering

OpticalEngineering.SPIEDigitalLibrary.org

Overview of self-mixing interferometer applications to mechanical engineering

Silvano Donati
Michele Norgia

SPIE.

Silvano Donati, Michele Norgia, "Overview of self-mixing interferometer applications to mechanical engineering," *Opt. Eng.* **57**(5), 051506 (2018), doi: 10.1117/1.OE.57.5.051506.

Optical Engineering 57(5), 051506 (May 2018)

REVIEW

Overview of self-mixing interferometer applications to mechanical engineering

Silvano Donati[a] and Michele Norgia[b,*]
[a]University of Pavia, Department of Industrial and Information Engineering, Pavia, Italy
[b]Politecnico di Milano, Department of Electronics, Informatics and Bioengineering, Milano, Italy

Abstract. We present an overview of the applications of self-mixing interferometer (SMI) to tasks of interest for mechanical engineering, namely high-resolution measurement of linear displacements, measurements of angles (tilt, yaw, and roll), measurements of subnanometer vibrations, and absolute distance, all on a remote target—representative of the tool-carrying turret of a tool-machine. Along with the advantages of SMI—compactness, low cost, minimum invasiveness, ease of use, and good accuracy, we illustrate the typical performance achieved by the basic SMI sensors, that is, the versions requiring a minimum of signal processing and discuss special features and problems of each approach. [DOI: 10.1117/1.OE.57.5.051506]

Keywords: optics; photonics; laser diodes; optical feedback; interferometry; metrology; measurements.

Paper 171694SSV received Oct. 25, 2017; accepted for publication Feb. 1, 2018; published online Mar. 1, 2018.

1 Introduction

Optical measurements methods for mechanical metrology dates back to 50 years ago,[1] when Hewlett–Packard introduced the famous Laser Interferometer HP5525 based on a He-Ne frequency stabilized laser used as the source of a modified Michelson optical interferometer employing corner cubes in place of mirrors.[2] With a $\lambda/8 \approx 79$-nm resolution over the full dynamic range of measurement extending to several meters,[2] the instrument soon became a workhorse for mechanical workshop calibrations of machine tools, with a sale volume (unverified) of several thousands per year.

Applications of the laser interferometer then flourished, mostly on displacement measurements, for the calibration of tool-machines to correct wear-out errors, and extensions were introduced to measure derived quantities such as planarity, angles, and squareness (See Ref. 2, Sec. 4.2.3).

An impressive three-axis simultaneous measurement with a single laser source was also reported (See Ref. 2, 4.2.3),[3] see the universal machine in Fig. 1. Yet, contrary to expectations, the X, Y, Z positioning with the "Laser Interferometer" did not become a massively deployed application, because of the advent of another optical technology, that of optical rules[4] much cheaper than the $50k class instrument, and yet adequate to supply the desired 0.4-mil or 0.01-mm resolution required in most metal-working applications.

So, it appeared that a sophisticated measurement instrument—the laser-based interferometer—had lost the competition for mechanical positioning and was confined to the yet rich field of calibration.

However, a breakthrough appeared in the midnineties with the introduction of the self-mixing interferometer (SMI),[5] the semiconductor laser version of a He-Ne SMI precursor first reported 10 years earlier.[6]

*Address all correspondence to: Michele Norgia, E-mail: michele.norgia@polimi.it

Indeed, on using a Fabry–Perot laser diode, the SMI provides a very compact, fraction-of-wavelength resolution interferometer, which, at the expense of a much reduced precision (three-digit in place of the typical seven-digits of a He-Ne stabilized laser), can cost even less than an optical rule and provide noncontact, minimum invasiveness.

In addition, with the introduction of the bright speckle tracking (BST) technique[7] capable of removing the amplitude fading of the signal returning from a diffuser,[8–10] the SMI technology was demonstrated capable of operating on a nonreflective optical surface, thus dispensing with the corner cube at the target side as needed for conventional laser interferometers.

Other recent advances have also encouraged the SMI application in the field of mechanical measurements. They have been: (i) the availability of cheap DFB lasers ensuring long term sub-ppm accuracy in wavelength[11] also at eye-safe wavelength (≈1500 nm with power lower than 10 mW); (ii) further to removal of amplitude fading, the analysis of the phase statistics of the returning signal due to speckle pattern, with the supportive result[12,13] that phase error can be kept well below the specifications of metal-working provided certain conditions on spot size and distance (discussed in Sec. 2) are met.

Thus, the measurement of (linear) displacement of the target is nowadays feasible with a cheap laser SMI yielding μm-resolution on a range of a few meters and operation on a plain untreated target surface.

Another measurement task demanded by tool-machine applications is that of determining the attitude of a tool-carrying turret, that is, measuring the three angles roll, pitch, and yaw. Actually, we may need up to 12 quantities for the complete spatial description[14,15] of the turret carrying the working tool of a machine: three positional quantities and three attitude angles for each axis. If adequate off-axis rigidity is assumed, then a five-axis NC machine[14,15] requires three position (X, Y, Z) and two attitude angles (pitch and yaw) measurements.[15]

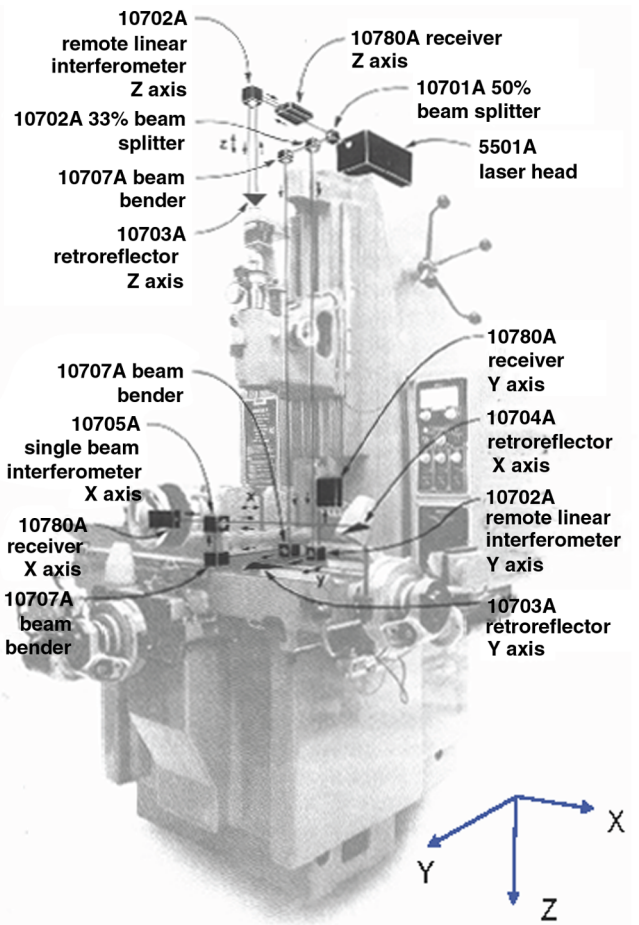

Fig. 1 A universal tool machine equipped with a Hewlett–Packard three-axis laser interferometer (See Ref. 2, Sec. 4.2.3).[4]

Angles are traditionally measured by a laser interferometer aiming to a bracket carrying two corner cubes with a transversal separation L, yielding a typical resolution of $\lambda/4L \approx 0.32$-arcsec (for $L = 100$ mm) (See Ref. 2, 4.2.3). With the SMI, the angle of a reflective plane target surface is measured by applying a minute transversal modulation to the small collimating lens of the laser diode and phase-detecting the resulting self-mixing signal.[16] Adequate resolution, typical 0.2 arcsec on a dynamic range of 5 arcmin has been obtained.[17]

More recently, it has been noted that two angle signals may coexist with the displacement signal in a single SMI channel;[18] basically, a single laser diode SMI can supply displacement, tilt, and yaw (see Fig. 2).

The third angle, that is roll, requires an optical element changing its optical path length upon rotation, for example, a quarter-wave plate interrogated by a traditional laser interferometer.[19] It is of course possible to think of an SMI readout of path length generated by roll; however, this scheme has been not yet developed experimentally.

Connected to the angle measurement is the operation of alignment of items, also a very frequent task for mechanical applications. The same configurations of angles can be used, both traditional and SMI, with typical accuracy that can go down to 0.2 arcsec. (Incidentally, this is an example of the superresolution offered by interferometry, because in the setup there is no aperture as large as the $12''_{\text{cm}}/0.2'' = 60$-cm diffraction limit would imply.)

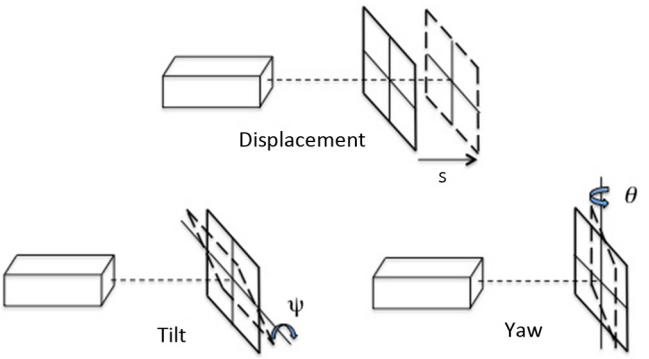

Fig. 2 Displacement and tilt ψ and yaw θ angles are measured simultaneously from the SMI signal.[19]

Next, vibration measurements are traditionally accepted as a powerful diagnostic tool for testing mechanical structures. As a terminology, we use vibration as the term describing the measurements of periodic very small (usually much less than λ) oscillations, in opposition to displacement which is for large aperiodic law of motion with dynamic ranges up to meters and moderate resolution (fraction of λ's). Another difference is that vibrations will be preferably measured by analog processing of the SMI signal,[20] whereas displacements are based on counting fringes or periods of the SMI, a digital processing.

Of course, the performances of digital versus analog and of vibration versus displacement measurements are rather different. Figure 3 shows the basic classification of SMI schemes, and typical performances obtained with SMI[21] (and also by traditional interferometry) through a Wegel's diagram: amplitude of displacement is plotted versus bandwidth (or frequency of vibration). The included area represents the measurement capability of the considered instrument, for digital and analog handling of the signal.

Vibration measurements can generally be applied to sense the mechanical transfer function of structures, from very small sizes—like that of a MEMS chip[22]—to very large, like that of a giant machine tool or also of towers and buildings.[23,24]

To develop an analog SMI vibrometer, a feedback loop technique has been introduced,[25] by which the working point of the SMI is locked at half-fringe, by amplifying the SMI signal, comparing it with the half-fringe level, and feeding the error difference to the laser diode supply current. In this way, minimum vibration amplitudes down to $50\ldots100\text{-pm}/\sqrt{\text{Hz}}$ have been measured[26] and, due to the feedback loop, the dynamic range is increased (from the initial $\lambda/2$ value) by a factor equal to the feedback loop gain, reaching to a wide dynamic range of millimeters.[26]

An interesting extension is that of the differential vibrometer,[26] made by two SMIs used as two channels the output signals of which are subtracted electronically, so that we can cancel a large common-mode amplitude of vibration and unveil the small differential one. In this way, we were able to demonstrate the optical, noncontact measurement of the mechanical hysteresis cycle of a sample (specifically, a damper bead of a motor).

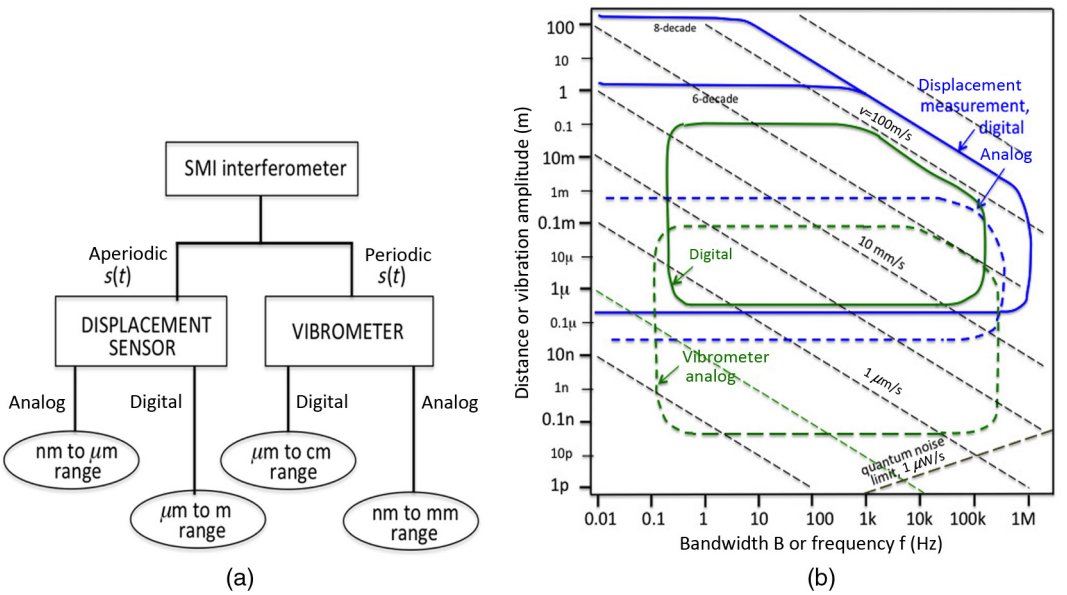

Fig. 3 Classification of (a) SMI schemes and (b) the range of performances for displacement and vibration SMI measurements, analog, and digital.[17]

Last but not least, by sweeping the drive current of the laser diode, we can develop an SMI performing absolute distance measurement.[27,28] This is different from the above-described displacement measurement, one incremental as it requires that fringes (or $\lambda/2$ pulses) are counted and accumulated to give the current displacement. By sweeping the laser current, we get a wavelength-sweep during which N new fringes are accommodated down the distance to be measured. Each new fringe is a $\lambda^2/2\Delta\lambda$step,[27,28] where $\Delta\lambda$ is the wavelength sweep we are able to impart to the laser diode, and distance is found as $L = N\lambda^2/2\Delta\lambda$, albeit no more with the fine interferometric $\lambda/2 \approx 0.4$-μm resolution but with a much coarser unit, typical $\lambda^2/2\Delta\lambda \approx 1\ldots3$ mm, that then can be brought to some $50\ldots100$ μm by averaging[28] or employing frequency estimation techniques.[29]

The four basic measurements outlined above can be considered as the building blocks of many additional applications, in mechanical engineering as well as in other field of physical measurements and of biology or medicine.[21] For example, the basic displacement scheme can be finalized to: (i) the real-time measurement of ablation depth[30] and (ii) become a velocimeter[31] when we look at the frequency content of the interferometric phase measured by the SMI, $\phi = 2\ ks$, ($k = 2\pi/\lambda$ being the wavenumber) whose time derivative $\mathrm{d}\phi/\mathrm{d}t = 2\ k\mathrm{d}s/\mathrm{d}t$ is just proportional to velocity, and also (iii) a flow meter[32–35] when we aim to a fluid in flow in front of the SMI, and (iv) a thickness meter.[36,37] Further applications have been successfully demonstrated and, for sake of saving space, we address the reader to a review paper[38] on SMI for a more exhaustive overview.

All the above applications witness the maturity of SMI as a viable technology in measurement science while the theoretical counterpart is provided by the Lang and Kobayashi equations,[39] a firm theoretical basis to describe SMI features and properties.

In the following sections, we describe the above-mentioned four measurements in more detail, to summarize their instrumental development and also to hint a crucial point about their development and performance. We assume that the reader is familiar with the basics of SMI, like that provided by a recent tutorial.[40] About the laser sources suitable to develop an SMI design in any of the four mentioned measurements, in principle any single longitudinal mode laser will be adequate, better if the (stray) side modes are at least 40 dB below the oscillating mode. Good specimens reported in past papers, all incorporating a monitor photodiode are the HL 8325 and the ML 2701, now discontinued, and the HL 7851 also discontinued but second sourced. The VCSEL PH85-F1P1S2-KC provides a good SMI signal at low (mA's) drive current, whereas the WSLD-1550-020m-1-PD is a DFB laser at the eye-safe wavelength.

2 Development of Displacement Measurement

To implement a displacement measurement SMI, we have to do nothing else that using a single-mode laser diode (LD) with an internal photodiode (PD) and mount it with a front objective collimating the emitted beam into a mm-size spot propagating to the target. The PD output current, amplified by a transimpedance amplifier, is the phase $\phi = 2\ ks$ carrying signal, undergoing a full-cycle 2π-swing every $\Delta s = \lambda/2$ increment of displacement s.

Usually, the (power) attenuation A along the propagation path is such that the strength parameter[38] C is larger than 1, where it is $C = (1+\alpha^2)^{1/2} A^{1/2} s/nL_d$ and α is the linewidth enhancement factor of the laser and nL_d its optical cavity pathlength.[38]

For $C > 1$, we have an SMI waveform like that shown in Fig. 4, a distorted sinusoid exhibiting a switching every 2π-period of phase ϕ (or $\lambda/2$ of displacement change). We limit C to <4.6 to avoid double and multiple switching per period,[5,38] and this requires a dynamical control of returning power level. The processing of SMI signal is straightforward (Fig. 5): switching is converted in a short pulse, which carry the polarity of target speed,[41] so that by time-differentiation and up/downcounting of pulses we get the displacement of the target in real-time. This mode

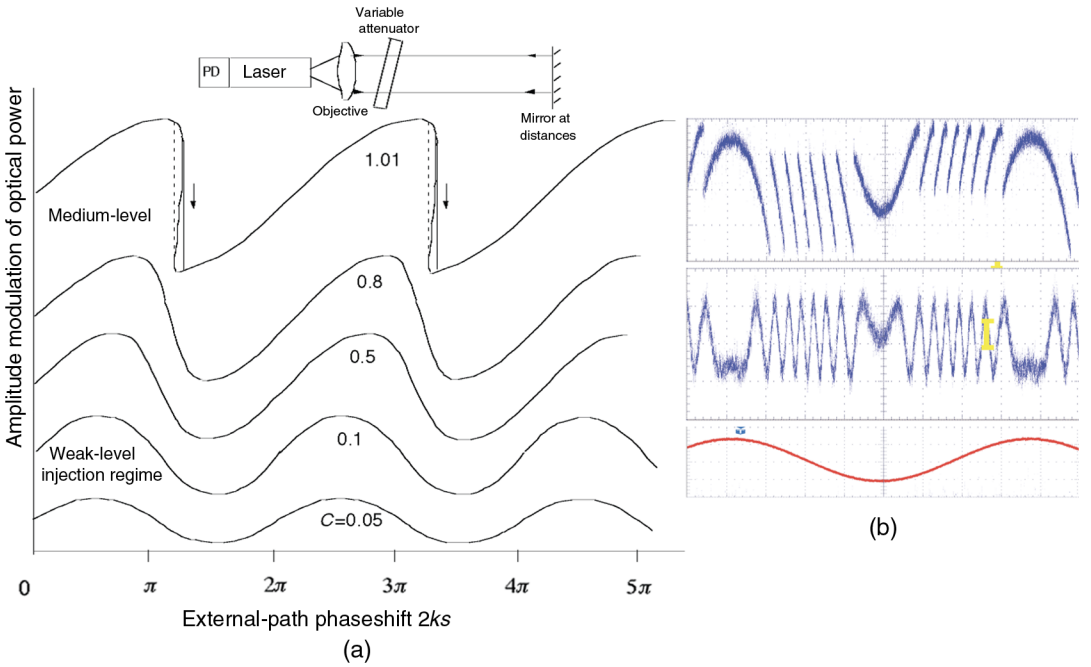

Fig. 4 (a) Calculated SMI waveforms at various C versus $\phi = 2ks$, and (b) measured SMI signal cos ϕ (top) for $C = 0.5$ and 1.5, along with the driving signal $\phi = \phi_0$ cos ωt (bottom).

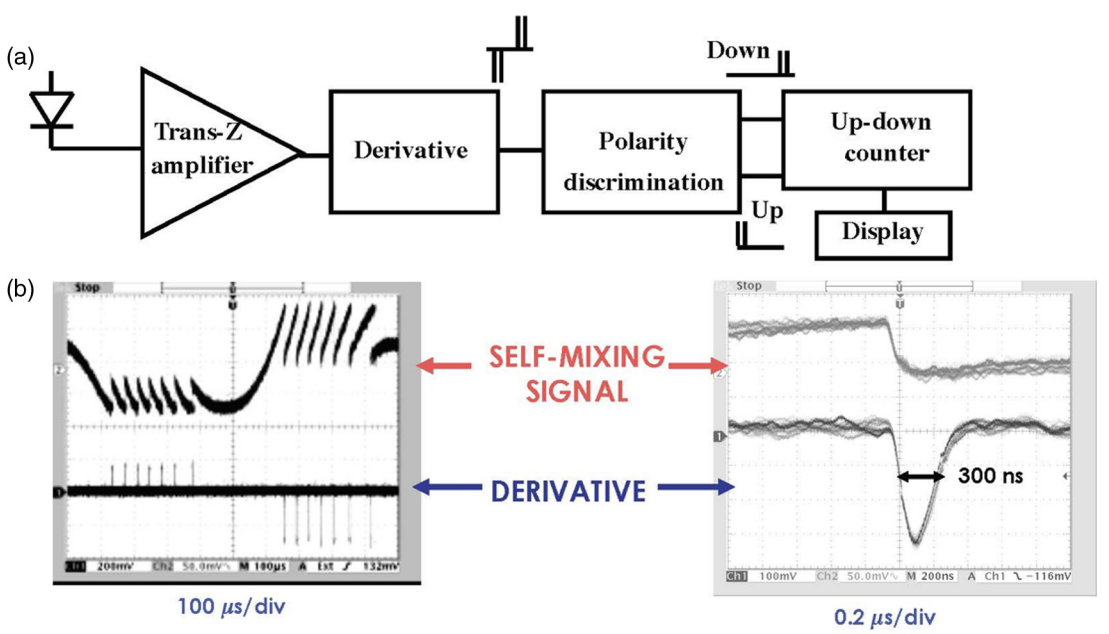

Fig. 5 (a) Electronic processing of SMI signal: after a transimpedance amplification, a time-derivative of the signal provides the $\lambda/2$ pulses, which are sorted according their polarity and dynamically counted in an up/downcounter, which records the displacement in $\lambda/2 = 400$-nm units. As pulses are shortened to 300-ns duration (b), maximum speed of target attains 400 nm/300 ns = 1.3 m/s.

of operation is clearly digital, with counting units of $\lambda/2 =$ 400 nm (for an 800-nm laser) and maximum speed determined by the pulse duration (300 ns in Fig. 5) as 400 nm/300 ns = 1.3 m/s, good enough to follow a fast turret movement.[42–48] Distance of operation depends on the laser diode and is however in the range of 0.5 to 2 m for a plain, white diffuser surface target.

About accuracy and precision of the measurement, wavelength stability is the first issue. Careful control of bias current and of temperature allows us to work with a stability down to the ppm (10^{-6}) level in the laboratory environment. Another issue is the speckle pattern statistics, adversely affecting amplitude of the SMI signal and introducing phase errors.[12,49]

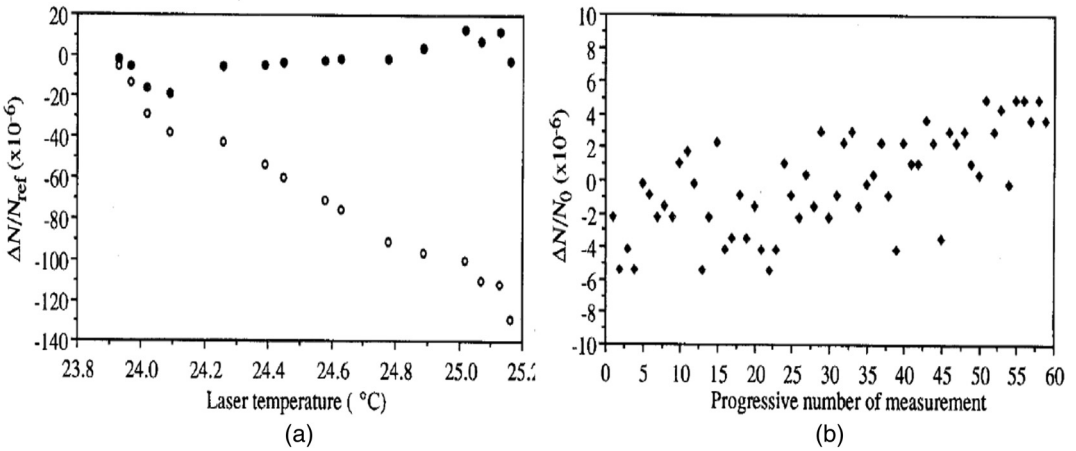

Fig. 6 Results of $s = 65$-cm displacement measurement exhibit a thermal roll-off (a, open circles), but after temperature is stabilized by a thermoelectric cooler, data return around zero (a, full dots). (b) The spread over $N = 60$ sample of measurements lasting 4 h is about ± 2 ppm.

To evaluate the intrinsic performance of the SMI, we have carried out set of repeated measurements on an $s = 65$-cm displacement. To avoid speckle errors, measurements were done on a corner cube target. First, as reported in Fig. 6(a), we observe an important roll-off with temperature, with a relative rms error $\Delta s/s$ of about -95 ppm/°C (1-ppm $= 10^{-6}$), just the thermal expansion coefficient of the aluminum table on which the experiment was sitting. But, after stabilizing the laser chip temperature with a thermoelectric (Peltier cell) cooler, data go around the zero-line with a spread of about 2 ppm on a set of 60 samples in a 4-h period,[37] see Fig. 6(b).

Actually, in the practical implementation of the displacement SMI, Fabry–Perot lasers fall short of the ppm-level resolution, because they exhibit wavelength mode-hopping at warm-up after switch-on, with a concurrent hysteresis. Instead, DFB laser should be employed, as these sources have been found capable of ensuring a ppm long term (>1 year) accuracy, at least in the laboratory. With the right laser diode, the SMI performance is thus comparable to that of a traditional He-Ne-based instrument.[37]

Now we want to go further and replace the corner cube with a plain diffuser as permitted by the SMI configuration [whereas this is unwieldy in a normal He-Ne-based interferometer (See Ref. 2, 4.2.3.4)]. The problem now is that speckle pattern statistics affects amplitude and phase of the field returning into the laser cavity,[49] just the field giving rise to the SMI effect.

An analysis of the phenomenon[12] shows that, while the phase error can be kept relatively small (e.g., a few μm's on $s = 1^{-m}$ swing), amplitude fluctuations are a serious problem and shall be strongly reduced, because they cause the loss of the signal (or a decrease below the desired $C > 1$ level) and of the associated $\lambda/2$ countings. This happens when we fall on a relatively "dark" speckle during the displacement of the target along the path $s(t)$ under measurement. More precisely, the probability of getting a speckle amplitude less than k (e.g., 0.01) times the average is just k (See Ref. 2, Sec. 5.2.1.). So even introducing an automatic gain control on a range G, there is always a small probability of fading, i.e., of signal becoming so small to be lost (e.g., a probability $0.01/G$).

One idea for mitigating speckle fading is to take advantage of the statistics itself: alongside a dark speckle there are probably other more intense, brighter speckles. If we arrange a minute deflection of the spot projected onto the target, large enough to change the speckle sample but small enough to leave the distance under measurement unchanged, we may be able to move away from the "dark" speckle fading and return to a sufficiently large return signal.

The deflection can be performed by a pair of small PZT piezoactuators holding the objective lens and moving it along the X-Y axes, and a servo circuit that, after the detection, closes the loop and feeds the piezo so as to keep the SMI signal maximized.[7]

The technique is called BST, and an example of the results is shown in Fig. 8, where, under a normal working condition, a "dark" speckle was found between $s = 74$ and 78 cm, with amplitude becoming so small that counts were lost. With the BST circuit on, the dip at 76 cm is avoided, and counts are registered correctly. (We can also see in Fig. 7 a stepup at about $s = 73.5$ cm where the system decides to jump to a brighter adjacent speckle.)

To be rigorous, also with BST we get a reduction but do not completely eliminate fading. Yet, as we may go down to a value $\approx 10^{-6}$ from $k = 0.01$, we make the SMI-BST instrument operation on a plain noncooperative diffuser acceptable from the practical point of view, with meter-swing capability and $\lambda/2$ resolution.[7]

Once fading is cured with the BST, the speckle statistics will affect the measurement because of the random phase added to the useful term $2ks$. An analysis of the phenomenon[12] shows that the speckle-related phase-error σ has two trends, called intra- and interspeckle cases, according to whether the displacement Δ (or Δs) under measurement is smaller or larger than the longitudinal speckle size $s_l = \lambda(2z/D)$,[2] s being the target distance and D is the diameter of the laser spot. The interspeckle is the case of displacement measurements, because usually the swing of the target can cover almost all or a large part of the dynamic range available. The results of the statistical analysis[12] are shown in Fig. 8, where we plot the noise-equivalent distance, noise equivalent displacement (NED) $= \sigma/2k$ (that is, phase reported to a distance error). (The other case, intraspeckle,

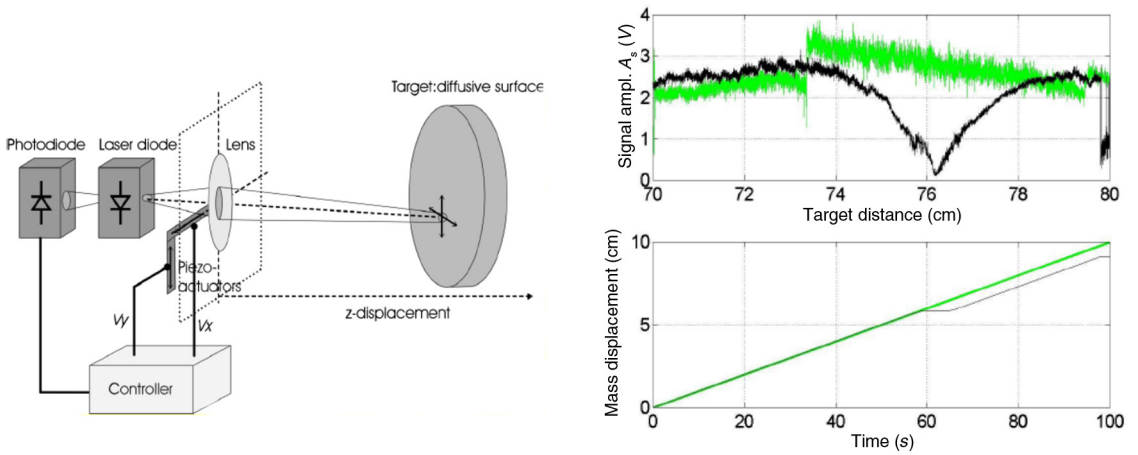

Fig. 7 (a) The technique called BST consists in moving slightly the objective lens along the *X* and *Y* axes by a pair of PZT actuators, so as to track the local maximum of intensity scattered by the diffuser back into the laser. (b) In an experiment demonstrating BST control, a dark speckle affecting a counting loss at $s = 76$ cm is avoided and the corresponding error is removed.

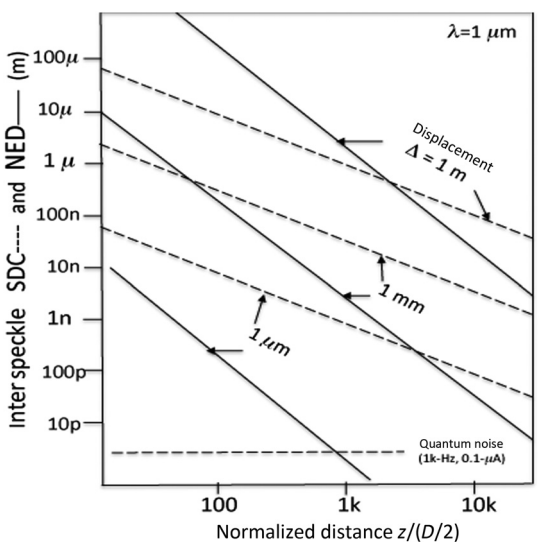

Fig. 8 Interspeckle phase error for a measurement on a large displacement Δ [larger than the longitudinal speckle size $\lambda(2z/D)^2$]: the NED error is plotted as a function of distance to spot-size ratio $z/(D/2)$ and with Δ as a parameter: due to the large Δ, also a systematic error (due to wavefront curvature changes), SDC, is found (dotted lines).

will be pertinent to vibrometer measurements and considered later.) Additional to the statistical error, we shall also consider a systematic error due to the wavefront curvature change upon the displacement we are measuring. The SDC—systematic displacement-error correction[12]—is also plotted in Fig. 8 with dotted lines.

As we can see from Fig. 8, both NED and SDC can be kept small, even for a large $D = 1$-m displacement, by using a small spot size $D/2$ so that $z/(D/2)$ is large enough for the desired Δ.

In conclusion, the above results show that state-of-the-art operation of a displacement-measuring interferometer and, in particular of an SMI, can be achieved on diffusing-like targets, up to meters distance and with a speckle error of the order of magnitude of λ.

A recent advance[50–52] has supplied a further contribution easing the development of fringe-counting operation of the SMI displacement measurement: by converting the frequency modulation of the SMI into an amplitude modulation by means of a steep edge filter, both cos $2ks$ and sin $2ks$ signals are available form the SMI and counting half- or quarter-periods can be done like in a conventional interferometer (See Ref. 2, 4.2.1), dispensing from the need of operation in the $1 < C < 4.6$ range necessary when we have available only one signal (i.e., the AM cos $2ks$).

3 Development of Angle Measurement

Since the early times of SMI, it has been observed that a reflection back into the laser from a remote mirror was well detectable even without applying any external excitation, because the microphonic-induced vibrations collected from the ambient already produce a sizeable SMI signal. This circumstance was employed as early as 1980 by Matsumoto,[53] who was able to align a He-Ne infrared laser to an external remote mirror, down to $\alpha \approx \pm 3$ arcsec angular error, just looking at the amplitude of the microphonic SMI signal. However, as the signal reaches a maximum when the alignment is the best and then rolls off with increasing angular error, the measurement response is nearly parabolic versus the angle α. In addition, the maximum range of measurement (or, the dynamic range) was rather limited, to a few arcmin.

An improved version[17] was presented by Giuliani et al., based on introducing a minute modulation of the angular direction of the laser beam, obtained by a piezoactuator moving transversally the collimating lens of the laser (Fig. 9). By comparing the phase of the SMI signal to the piezodrive, a phase detection that transforms the parabolic dependence into a linear one was obtained.

[Of course, different from the other SMI measurements, for the angle measurement the target shall be a reflective (not a diffusive) surface.]

With conventional nonoptimized components, noise-limited resolution of ≈0.2 arcsec and dynamic range up to

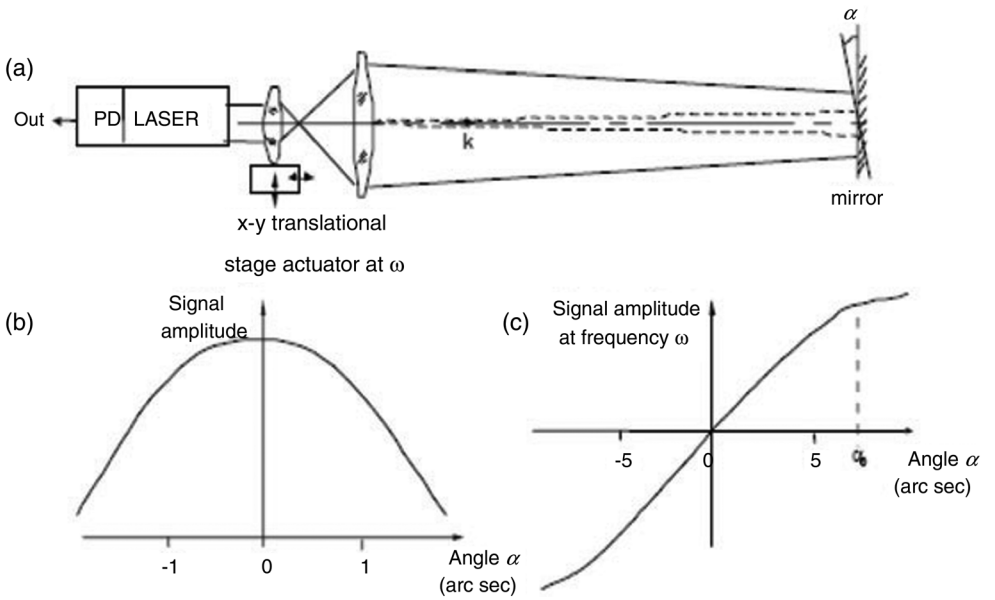

Fig. 9 Angle measurement with SMI: when the remote mirror is well aligned, the SMI signal due to ambient microphonics is maximized (b). In an improved setup (a), we modulate the angle by an XY piezoactuator that slightly moves the objective lens. The resulting SMI signal is sensed in amplitude and phase respect to the drive signal ($\pm$ sign for phase/antiphase). (b) The parabolic-like response curve is thus transformed in (c) a quasilinear passing through the zero.

≈5 arcmin have been demonstrated,[17] the performance of a very good autocollimator.

Recently, the angle measurement has been extended[18] to two components of the attitude placement of the target, namely pitchψ and yaw θ, like indicated in Fig. 2.

Indeed, on using orthogonal drive functions to actuate the piezodrive along the X and Y axes (such as sin and cos), we can read and then recover simultaneously without crosstalk the signals of the two angles ψ, θ, and have them modulate the normal (displacement) $2ks$ signal of the SMI, see Fig. 10.

Interesting for machine tool applications, the two angles can then be measured together with the normal interferometric signal related to displacement because of the different frequency content, just using a single signal channel,[18] see the example of Fig. 10.

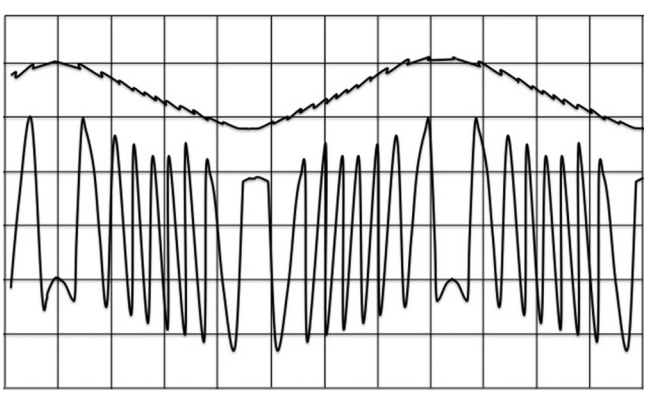

Fig. 10 Displacement and two angles (tilt and yaw) can be measured simultaneously with a single channel SMI signal (right); angle signal (top) and displacement signal (bottom) are produced by a pivoted slab put into vibration. The different frequency content of angles and displacement signals allows to separate them easily.

About the third component of attitude, namely the roll, which is an in-plane angle, a more complicated configuration is needed, because we need to transform roll into an out-of-plane phaseshift.[19]

4 Development of Vibration Measurement

On measuring periodical motion of small amplitude and a frequency range—say from audio to MHz—counting $\lambda/2$-steps is too rough and we may prefer an analog processing. To start with, the analog format has a dynamic range limitation—a typical op-amp circuit can accommodate signals ranging from mV's (the offset limit) to tens of volts, or have a 10^4 dynamic range—thus, two or three decades less than digital processing in a displacement interferometer with 6…7 decades. There is room, however, to significantly improve sensitivity to small displacements, well beyond the $\lambda/2$-limit, and approach the quantum noise limits of detected signal.

Indeed, the minimum detectable displacement or noise equivalent displacement is easily found (See Ref. 2, Sec. 4.4.5.) by noting that the detected signal $I_{ph} = I_{ph0}(1 + \cos\phi)$ where $\phi = 2ks$ has maximum sensitivity to phase at the half-fringe point (at $\phi = \pi/2$) where $(\Delta I_{ph}/I_{ph0})^2 = (\phi)^2$. Recalling the expression for the shot noise associated with the detected current, that is $(\Delta I_{ph})^2 = 2\,eI_{ph0}B$, we readily get $\langle(\Delta\phi)^2\rangle = 2\,eB/I_{ph0} = \mathrm{SNR}^{-1}$, where SNR is the signal-to-noise ratio of the amplitude (i.e., photocurrent) measurement. Using $\Delta\phi = 2k\Delta s$ gives:[43] $\mathrm{NED} = \langle\Delta s^2\rangle^{1/2} = \lambda/2\pi[eBI_{ph0}]^{1/2} = \lambda/4\pi\mathrm{SNR}^{1/2}$. Putting numbers reveals that the minimum detectable displacement can go down to nanometers for detected currents of μA's and bandwidth of MHz and even to picometers for mA's and kHz. These limits are reached or approached substantially in practice, provided we first cure a number of much larger sources of disturbance and interference

commonly found in the experiment and in circuits processing the signal.

Now, there are basically two approaches to implement a small-signal vibrometer by analog-signal processing, that is

i. Readout at half-fringe,[25,26] so as to take advantage of the linear conversion offered by the phase-to-current relationship when the interferometer is read in quadrature. To this end, we shall set the quiescent working point of the SMI in the middle of the cosine amplitude swing, around $\phi = \pi/2$. Indeed, letting $\phi = \pi/2 + 2ks$, the signal is $I_{ph} = I_{ph0}(1 + \cos\phi) = I_{ph0}(1 - \sin\phi) \approx -I_{ph0}\phi$ for small ϕ. Then, for small displacements $\Delta I_{ph} = -I_{ph0}\Delta\phi = -I_{ph0}2k\Delta s$, i.e., we get a linear relation between Δs and the SMI output signal, and we can read $\Delta s = \Delta\phi/2k$ directly from the current variations ΔI_{ph} of the detected current. Note that the linear range of response is limited to $\pm\lambda/2$ by the cosine-like function, at least in the basic arrangement. This technique, known since the early times of conventional interferometry, is easy to implement when a reference arm is available, because the half-fringe condition is in this case written as $\cos(\phi_{meas} - \phi_{ref}) \approx 0$, or, we shall adjust the reference pathlength to be $\phi_{ref} = \Delta\phi_{meas} + \pi/2$, so that $\cos(\phi_{meas} - \phi_{ref}) = -\sin\Delta\phi_{meas} \approx -\Delta\phi_{meas}$ for small $\Delta\phi_{meas}$.
ii. Waveform reconstruction technique.[54–56] We can solve for $s(t)$ from the measured photocurrent $I_{ph}(t)$, by inverting the general relationship $I_{ph} = I_{ph0}[1 + F(2ks)]$ for $0 < 2ks < 2\pi$, and then using an unfolding algorithm to extend the reconstruction[55] for $N2\pi < 2ks < (N+1)2\pi$. In principle, this method can reconstruct $s(t)$ on a relatively large number N of periods, only limited by the accuracy with which parameters C and α of the SMI are known.

In practice, results reported in literature are limited to $N \approx 30\ldots100$ or max amplitudes of $s = 50\ldots150\ \mu$m (peak-to-peak), whereas for small s the residual computational errors are or the order of $5\ldots10$ nm,[56] much larger than the noise limit attainable in case (i).

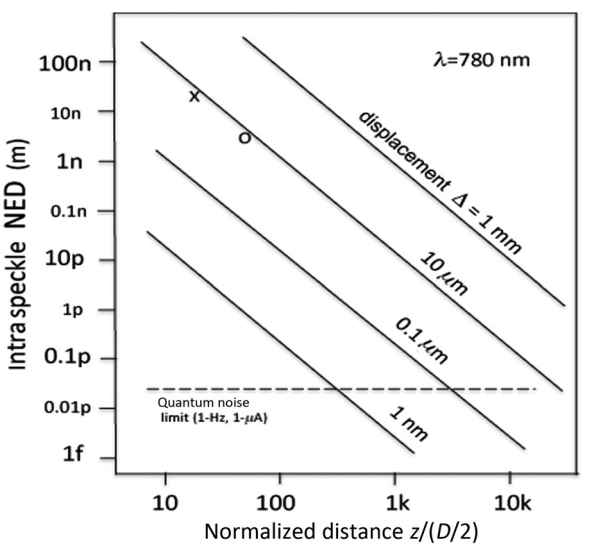

Fig. 11 The NED of intraspeckle phase error plotted versus normalized distance and with amplitude of vibration Δ as a parameter.

About operation on a plain, diffusing surface, also the SMI vibrometer suffers by the speckle-related amplitude fading and phase error. However, as the involved displacements are very small, the effects are much milder and can be tackled easily.[12]

Indeed, amplitude fading can be cured by simply moving away from dark speckle with a small transversal movement of the spot.

Phase error is much less severe than in displacement measurements, like indicated by the intraspeckle statistics analyzed in a recent paper,[12] and is represented in Fig. 11 in terms of NED versus normalized distance $z/(D/2)$ and with the vibration amplitude Δ as a parameter.

4.1 *Vibrometer with Half-Fringe Locking*

In an SMI, no reference is available to adjust the fringe signal in quadrature, but we can take advantage of the λ-dependence of the semiconductor laser from the bias current to develop a control loop and set the working point at half-fringe[25] of the interferometer. In the moderate feedback regime ($C > 1$), a fairly linear semiperiod of the fringe is available (Fig. 12) as the region of operation. To dynamically lock the working point at half fringe, consider the detected signal at the output of the transimpedance amplifier of the photodiode and its amplitude swing, and let V_{ref} be the half-fringe voltage. We use V_{ref} as the reference input of a difference op-amp (block of gain A in Fig. 12) receiving the detected signal $V_{op\text{-}amp}$ at the other input. Then, we amplify the difference and convert it to a current (block G_m) and send the current to feed the laser diode. As current I_{bias} impresses a wavelength variation $\Delta\lambda = \alpha\Delta I_{bias}$, and hence a wavenumber variation $\Delta k = -k\Delta\lambda/\lambda$, we have closed the feedback loop and servoed the phase $2ks$ signal.

Indeed, as the target moves and generates an interferometric phase $2k\Delta s$, the feedback loop reacts with a wavelength change yielding an equal and opposite phase $-2s\Delta k$. So, at the target we have an "optical" virtual ground keeping dynamically zero the error signal. By virtue of the feedback loop, the vibration signal $2k\Delta s$ now appears at the output V_{out} of the difference amplifier [Fig. 12(b)].

This rather surprising result is a consequence of a large loop gain, by which a small difference between V_{ref} and the op-amp output $V_{op\text{-}amp}$ will be exactly the one needed to generate V_{out} and from it the $\alpha G_m V_{out}$ bias current that satisfy the phase-nulling condition $2\Delta ks - 2k\Delta s = 0$. Thus, we get the vibration signal from the op-amp output as $\Delta V_{out} = [\alpha_\lambda G_m]^{-1}(\lambda/s)\Delta s$.

Interestingly, the result is independent from the amplitude of the photodetected signal I_{ph} and all its fluctuations, including target backreflection factor and speckle pattern fading.

The only condition is that the loop gain G_{loop} is large. From Fig. 12, loop gain is easily evaluated as $G_{loop} = \mathrm{RA}\,\alpha_\lambda G_m(s/\lambda)\sigma P_0$. In practice, in a typical layout,[25,26] we can have $G_{loop} \approx 500\ldots1000$, a condition close to ideality of large gain. More precisely, as a well-known consequence from feedback theory, we can say that residual nonidealities found in the closed loop reduced by a factor G_{loop} respect to the nonfeedback condition. In particular, speckle-pattern fading is nicely reduced by a factor $500\ldots1000$.

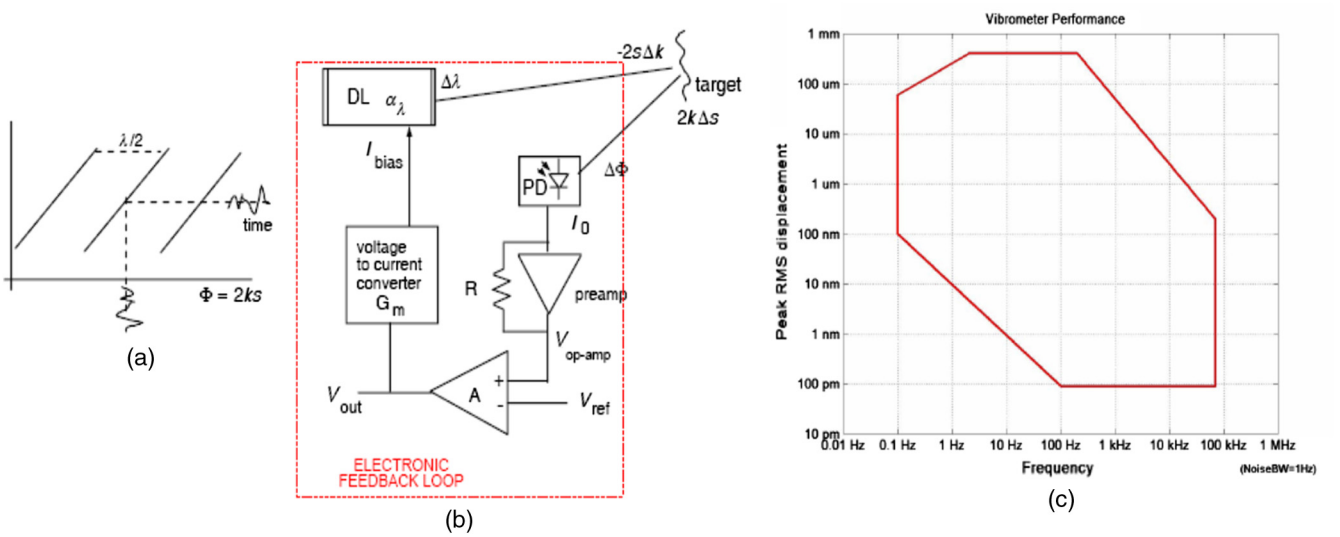

Fig. 12 (a) Half-fringe locked vibrometer: the quiescent point is locked at the middle of the signal swing (b) using a feedback loop made by a transimpedance amplifier, a difference amplifier, a voltage-to-current converter, and the I-to-λ dependence of the laser diode. By virtue of the feedback loop, $V_{\text{op-amp}}$ is locked to V_{ref}, and $2k\Delta s$ is locked to $2s\Delta k$. (b) The vibration signal $2k\Delta s$ is then found at the output V_{out} of the difference amplifier A. (c) Performance of the half-fringe locked vibrometer: minimum measured displacement is 100 pm ($B = 1$ Hz) and maximum amplitude 500 mm, frequency range is from 0.1 Hz to 80 kHz.

Another beneficial effect of the feedback loop is that linearity and dynamic range are improved by a factor G_{loop}.[25] As it is well known from control theory, the dynamic range limit is just an error introduced in the loop and as such is reduced by G_{loop}.

Thus, our small-signal vibrometer will not saturate as the vibration amplitude is larger than half fringe (or $>\lambda/2$). Indeed, as the signal increases and tends to slip out of the fringe, the feedback loop will pull it back, leaving only a $1/G_{\text{loop}}$ residual. So, the dynamic range becomes now $G_{\text{loop}}\lambda/2$, something in the range of $200\ldots500\ \mu$m, or even in the range of mm's with careful design.

An example of performances obtained with a breadboard vibrometer developed from the concept of half-fringe servo

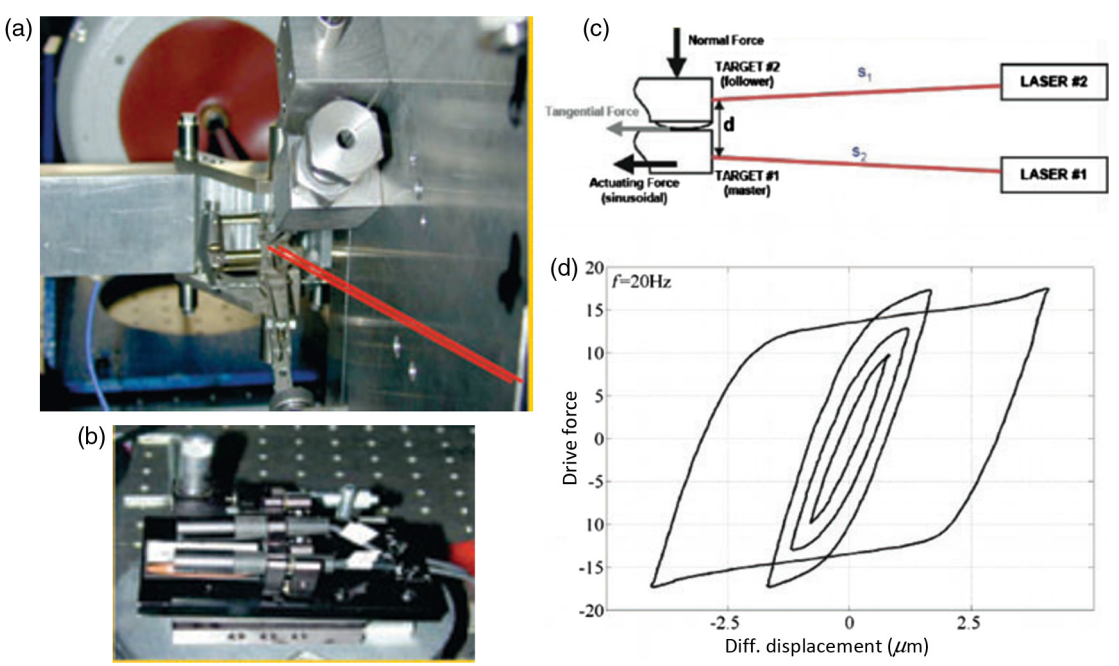

Fig. 13 Stress/strain measurement: (a) the shaker machine to test a braking bead (the two parallel beams point to bead and its basement); (b) the two differential vibrometer heads; (c) placement of the two vibrometer; (d) the stress/strain cycle is measured by the instrument, showing elastic regime with negligible hysteresis ($F < 7$ N peak), the plastic regime when the hysteresis loop opens up ($F = 8\ldots15$ N) and the bead dissipates energy, before the breakdown occurs (at about $F \cong 17.5$ N).

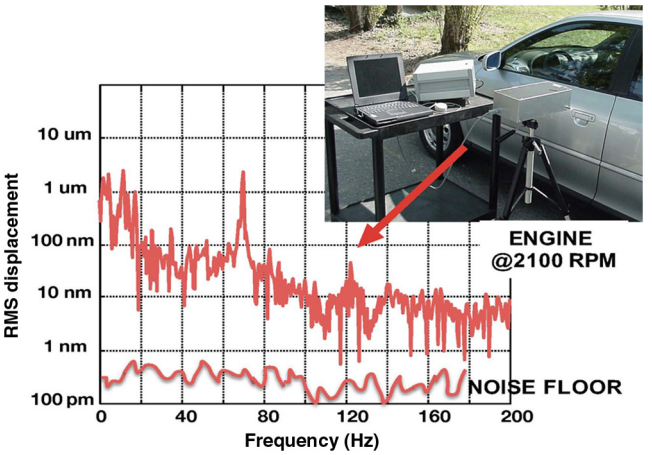

Fig. 14 Vibration response detected by the SMI vibrometer on the door of a car while the engine is on: a complicated pattern of modes, well above the noise floor, is detected, of interest for the diagnostic of the structure.

loop is reported in Fig. 12(c), showing a minimum detectable signal of NED = 100 pm (on $B = 1$-Hz bandwidth) and a maximum (dynamic range) of ≈500 μm.

Recently, a digital version for the electronic feedback loop was proposed,[57] able to optimize the feedback transfer function, due also to a careful system modeling.[58]

4.2 *Differential Vibrometer for Stress/Strain Hysteresis Cycle Noncontact Measurements*

The SMI vibrometer described in the last section lends itself easily to the differential mode of operation, what we need to measure small vibrations superposed to larger common-mode movements. In a normal interferometer, we take advantage of the usually available reference arm, so that we can measure[2] $(\phi_1 - \phi_2) = 2k(s_1 - s_2)$. But, if we want to work on diffuser-like target surface, the speckle statistics will introduce large amplitude fluctuations and make operation very unsteady.

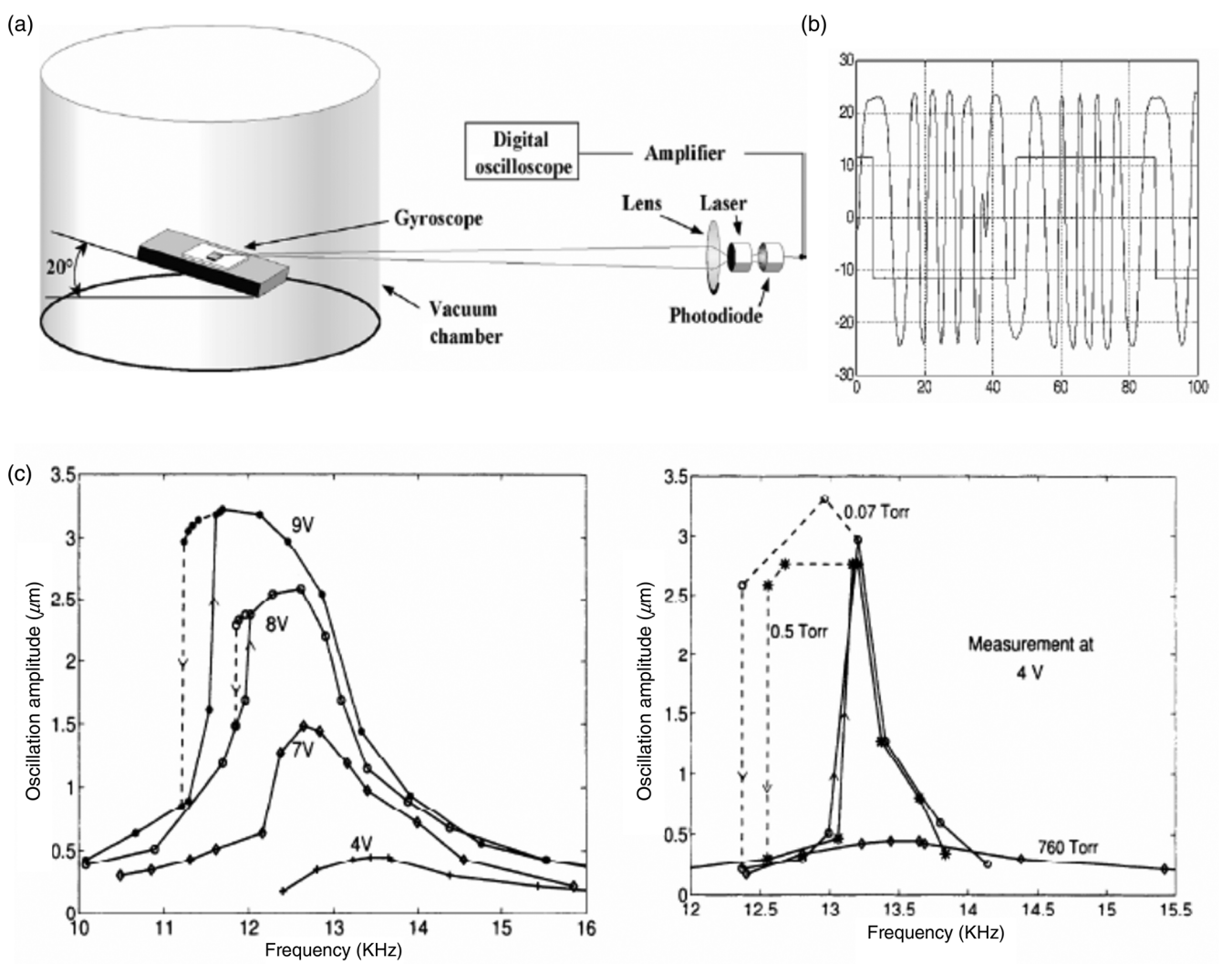

Fig. 15 (a) To test the electromechanical properties of Si-machined MEMS with SMI, the laser spot is focused on the minute vibrating mass of the chip through the glass wall of a vacuum chamber. The vibration of the mass is viewed at an angle (≈20 deg), and the appropriate correction is applied to the SMI fringe signal (b) giving the displacement waveform. (c) Counting the developed fringes easily brings to the frequency response at various level of voltage excitation and at different pressures.

Using the SMI half-fringe stabilized vibrometer with the phase signal internal to the feedback loop, we have removed the speckle fading as explained above, but we lack a second reference (optical) arm. However, as ΔV_{out} is a replica of phase $\phi = k\Delta s$, we may think of subtracting electrical signals instead of optical phases. So, we make a double-channel SMI vibrometer, with one channel aimed to the common mode signal s_{CM}, and the other aimed to $s_{CM+}s_D$, containing the differential signal s_D.

After checking that two channels can be built with nearly identical performance (mismatch in responsivity <0.1%, noise floor and dynamic range differing by <5%),[26] we checked that the electronic subtraction differential behaves as well as the optical phase differential interferometer and deployed it to a mechanical test application.

Experiment was a brake-bead test bed (Fig. 13) in which a shaker excites a bead, fixed onto a base support, and reaching 800°C. The stress is a quasisinusoid V_{ST} excitation, and the support vibration is the s_{CM}, whereas the bead vibration is the differential s_D. The common mode was about $15\ldots30$ μm wide and the differential $0.5\ldots4$ μm.

From the point of view of mechanics, the V_{ST} excitation is proportional to the stress T, and the differential s_D is proportional to the strain S of our mechanical sample, so we are able to draw the stress/strain cycle for the first time.[26] As we can see from the result reported in Fig. 13(b), at moderate stress the sample is in the elastic or Newtonian regime, with a linear dependence of S from T and no hysteresis. At a certain threshold, the material enters the plastic regime and the diagram opens up with hysteresis. Note that the area of the cycle, integral of $T\mathrm{d}S$, is the energy dissipated per cycle, or the breaking efficacy of the bead used as a damper. Upon the increase in T, the hysteresis cycle widens until, on a little further increase in T, the sample finally breaks down (and curve disappears). The above information is of enormous value for the design and testing of mechanical structures, and the SMI vibrometer is the key instrument to measure it.

4.3 *Measurement of the Transfer Function*

One of the most interesting applications of the SMI vibrometer is the measurement of the transfer function of a mechanical system. The differential vibrometer of Sec. 4.2 for the detection of hysteresis cycle is an example of transfer function measurement. Anyhow, a single channel vibrometer is typically adequate to measure the response of a variety of mechanical systems. For example, on aiming the vibrometer beam on the door of a car,[25] we can find a rather complicated spectrum of response (see Fig. 14), when the engine motor is switched on.

On another scale, that of microcircuits, the SMI vibrometer is capable of measuring the frequency response of a MEMS, focusing the measuring beam on a 100×100-μm^2 chip[21] and obtaining the response diagram reported in Fig. 15.

5 Development of Absolute Distance Measurement

Like any interferometer, SMI provides an incremental measurement of distance, and we call it displacement because it requires moving the retroreflector from the initial $z = s_1$ to the final $z = s_2$ position to develop and count the incremental steps of phase variation $\Delta\phi = 2k(s_1 - s_2)$. At first sight, a nonincremental (viz., absolute) distance measurement looks outside the reach of a phase-based interferometer. Actually, phase variations $\Delta\phi = 2k\Delta s + 2s\Delta k$ are generated also by wavenumber variations Δk, not only by displacement increments Δs. So, the idea for an SMI absolute distance meter is that of sweeping wavelength (instead of moving the target) to develop counts of phase increments, as first proposed by Bosch et al.[59]

About resolution, the unit of distance measurement is $d_{unit} = \lambda^2/2\Delta\lambda$, so we shall look for a laser source providing a large $\Delta\lambda$ swing for best resolution. Commonly used laser Fabry–Perot laser diodes may have up to $\Delta\lambda = 0.2$ nm at $\lambda = 0.85$ μm, as limited by mode-hopping problems, however, resulting in a reasonable $d_{unit} = 1.8$ mm. The error

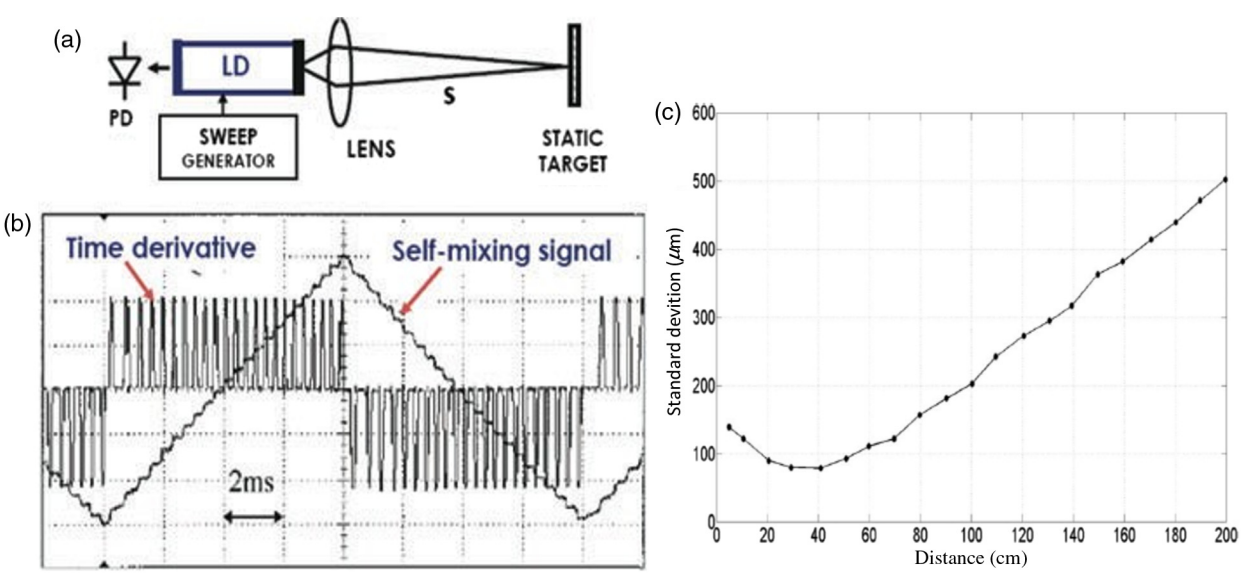

Fig. 16 Absolute distance measurement with an SMI: applying a bias current sweep to the laser diode (a), wavelength is modulated with a triangular waveform, and phase$\phi = 2ks$ exhibits a number N of 2π-periods variations of the SMI signal (the small ripple on waveform, b). The SMI signal is time-differentiated and d the periods N counted. Unit of scale distance is $\lambda^2/2\Delta\lambda$. (c) The spread of measurements on $s = 0\ldots2$ m distance.[29]

can, however, be made much smaller than the discretization step after appropriate averaging or feedback techniques.[27,60] An improvement in measurement performances[29,61] (resolution and measurement time) is obtained due to frequency estimation techniques, not limited by the fringe number quantization, such as the interpolated fast Fourier transform[62] or more complex algorithms.[63] Typically, an error of 0.1 to 0.5 mm on a distance 10 to 200 cm has been obtained,[29] as shown in the performance diagram reported in Fig. 16, representative of a real distance-measuring instrument.

The induced wavelength modulation, essential for distance measurement, allows for simultaneous speed measurement,[39] by direct estimation of the Doppler effect: it induces a frequency difference between the signals corresponding to the two sides of the triangular modulation (see Fig. 16). This technique is extremely robust against signal fading and directly applicable in industrial environment.[64]

6 Conclusions

We have presented an overview of the SMI technology and shown that it is conveniently applied to mechanical measurements. We have also tried to systematize the field of SMI measurements. The examples reported inevitably reflect the scientific interest of the authors, yet they are representative of basic ideas and tools we can deploy in R&D on SMI. We have illustrated the guiding principles and how methods and options from different disciplines (electronics, communication, control theory, etc.) can cross fertilize the SMI concepts, what really makes SMI an effective approach, quite different from the apparent simplicity of its basic setup. Self-mixing is still far from being fully exploited, and we think that, in the years to come, it will continue to offer an excellent opportunity for the activity of young researchers and a ground to make the most of creativity and talent.

References

1. F. Rude and M. J. Ward, "Laser transducer system for high accuracy machine positioning," *Hewlett Packard J.* **27**(6), 2–6 (1976).
2. S. Donati, *Electro-Optical Instrumentation—Sensing and Measuring with Lasers*, Prentice Hall, Upper Saddle River (2004).
3. R. C. Quenelle and L. J. Wuerz, "A new microcomputer controlled laser dimensional measurement and analysis," *Hewlett Packard J.* **4**, 4–13 (1983).
4. S. Donati, *Photodetectors*, Prentice Hall, Upper Saddle River (2000).
5. S. Donati, G. Giuliani, and S. Merlo, "Laser diode feedback interferometer for measurement of displacement without ambiguity," *IEEE J. Quantum Electron.* **31**, 113–119 (1995).
6. S. Donati, "Laser interferometry by induced modulation of the cavity field," *J. Appl. Phys.* **49**(2), 495–497 (1978).
7. M. Norgia, S. Donati, and D. d'Alessandro, "Interferometric measurements of displacement on a diffusing target by a speckle-tracking technique," *IEEE J. Quantum Electron.* **37**, 800–806 (2001).
8. R. Atashkhooei, S. Royo, and F. Azcona, "Dealing with speckle effects in self-mixing interferometry measurements," *IEEE Sens. J.* **13**, 1641–1647 (2013).
9. R. Kliese and A. D. Rakic, "Spectral broadening caused by dynamic speckle in self-mixing velocimetry sensors," *Opt. Express* **20**(17), 18757–18771 (2012).
10. U. Zabit, O. D. Bernal, and T. Bosch, "Self-mixing laser sensor for large displacements: signal recovery in the presence of speckle," *IEEE Sens. J.* **13**, 824–831 (2013).
11. R. S. Vodhanel, M. Krain, and R. E. Wagner, "Long-term wavelength drift of 0.01 nm/y for 15 free-running DFB lasers," in *Proc. OFC Optical Fiber Conf.*, San Jose, paper WG5, pp. 103–104 (1994).
12. S. Donati, G. Martini, and T. Tambosso, "Speckle pattern errors in self-mixing interferometry," *IEEE J. Sel. Top. Quantum Electron.* **49**, 798–806 (2013).
13. S. Donati and G. Martini, "Systematic and random errors in self-mixing measurements: effect of the developing speckle statistics," *Appl. Opt.* **53**, 4873–4880 (2014).
14. K. Harding, *Handbook of Optical Dimensional Metrology*, Chapters 3–5, CRC Press, Boca Raton (2013).
15. J. G. Webster and H. Eren, *Measurement, Instrumentation, and Sensors Handbook*, 2nd ed., Chapters 27–36, CRC Press, Boca Raton (2014).
16. S. Donati and M. Norgia, "Displacement and attitude angles (tilt and yaw) are measured by a single-channel self-mixing interferometer," in *Conf. on Laser and Electro-Optics (CLEO)*, San Jose, Paper AW4J1 (2016).
17. G. Giuliani et al., "Angle measurement by injection detection interferometry in a laser diode," *Opt. Eng.* **40**, 95–99 (2001).
18. S. Donati, D. Rossi, and M. Norgia, "Single channel self-mixing interferometer measures simultaneously displacement and tilt and yaw angles of a reflective target," *IEEE J. Quantum Electron.* **51**, 1400108 (2015).
19. J. Qi et al., "Note: enhancing the sensitivity of roll-angle measurement with a novel interferometric configuration based on waveplates and folding mirror," *Rev. Sci. Instrum.* **87**, 036106 (2016).
20. A. Jha, F. J. Azcona, and S. Royo, "Frequency-modulated optical feedback interferometry for nanometric scale vibrometry," *IEEE Photonics Technol. Lett.* **28**(11), 1217–1220 (2016).
21. S. Donati and M. Norgia, "Self-mixing interferometry for biomedical signals sensing," (invited paper) *IEEE J. Sel. Top. Quantum Electron.* **20**, 6900108 (2014).
22. V. A. Lodi, S. Merlo, and M. Norgia, "Measurements of MEMS mechanical parameters by injection interferometry," *IEEE J. Microelectromech. Syst.* **12**, 540–549 (2003).
23. M. Corti, F. Parmigiani, and S. Botcherby, "Description of a coherent light technique to detect the tangential and radial vibrations of an arch dam," *J. Sound Vib.* **84**, 35–45 (1982).
24. A. Miks and J. Novak, "Non-contact measurement of static deformation in civil engineering," in *Proc. ODIMAP III*, Pavia, pp. 57–62 (2002).
25. G. Giuliani, S. Bozzi-Pietra, and S. Donati, "Self-mixing laser diode vibrometer," *Meas. Sci. Technol.* **14**, 24–32 (2003).
26. S. Donati, M. Norgia, and G. Giuliani, "Self-mixing differential vibrometer based on electronic channel subtraction," *Appl. Opt.* **45**, 7264–7268 (2006).
27. M. Norgia, G. Giuliani, and S. Donati, "Absolute distance measurement with improved accuracy using laser diode self-mixing interferometry in a closed loop," *IEEE Trans. Instrum. Meas.* **56**, 1894–1900 (2007).
28. T. Bosch et al., "Three-dimensional object construction using a self-mixing type scanning laser range finder," *IEEE Trans. Instrum. Meas.* **47**, 1326–1329 (1998).
29. M. Norgia, A. Magnani, and A. Pesatorim, "High resolution self-mixing laser rangefinder," *Rev. Sci. Instrum.* **83**, 045113 (2012).
30. A. G. Dmir et al., "Evaluation of self-mixing interferometry performance in the measurement of ablation depth," *IEEE Trans. Instrum. Meas.* **65**, 2621–2630 (2016).
31. A. Magnani and M. Norgia, "Spectral analysis for velocity measurement through self-mixing interferometry," *IEEE J. Quantum Electron.* **49**, 765–769 (2013).
32. M. Norgia, A. Pesatori, and S. Donati, "Compact laser diode instrument for flow measurement," *IEEE Trans. Instrum. Meas.* **65**, 1478–1483 (2016).
33. L. Campagnolo et al., "Flow profile measurement in microchannel using the optical feedback interferometry sensing technique," *Microfluid. Nanofluid.* **14**, 113–119 (2013).
34. Y. L. Lim et al., "Self-mixing flow sensor using a monolithic VCSEL array with parallel readout," *Opt. Express* **18**, 11720–11727 (2010).
35. E. E. Ramírez-Miquet et al., "Optical feedback interferometry for velocity measurement of parallel liquid-liquid flows in a microchannel," *Sensors* **16**(8), 1233 (2016).
36. M. Fathi and S. Donati, "Thickness measurement of transparent plates by self-mix interferometer," *Opt. Lett.* **35**, 1844–46 (2010).
37. I. Xu et al., "Simultaneous measurement of refractive-index and thickness for optical materials by laser feedback interferometry," *Rev. Sci. Instrum.* **85**(8), 083111 (2014).
38. S. Donati, "Developing self-mixing interferometry for instrumentation and measurements," *Laser Photonics Rev.* **6**, 393–417 (2012).
39. R. Lang and K. Kobayashi, "External optical feedback effects on semiconductor injection laser properties," *IEEE J. Quantum Electron.* **16**, 347–355 (1980).
40. T. Taimre et al., "Laser feedback interferometry: a tutorial of the self-mixing effect for coherent sensing," *Adv. Opt. Photonics* **7**, 570–631 (2015).
41. S. Donati, L. Falzoni, and S. Merlo, "A PC-interfaced, compact laser-diode feedback interferometer for displacement measurements," *IEEE Trans. Instrum. Meas.* **45**, 942–947 (1996).
42. M. Norgia and S. Donati, "A displacement-measuring instrument utilizing self-mixing interferometry," *IEEE Trans. Instrum. Meas.* **52**, 1765–1770 (2003).
43. C. Bes, G. Plantier, and T. Bosch, "Displacement measurements using a self-mixing laser diode under moderate feedback," *IEEE Trans. Instrum. Meas.* **55**, 1101–1105 (2006).
44. D. Guo, M. Wang, and H. Hao, "Displacement measurement using a laser feedback grating interferometer," *Appl. Opt.* **54**(13), 9320–9325 (2015).
45. O. D. Bernal et al., "Robust fringe detection based on bi-wavelet transform for self-mixing displacement sensor," in *IEEE SENSORS* (2015).

46. U. Zabit et al., "Adaptive self-mixing vibrometer based on a liquid lens," *Opt. Lett.* **35**, 1278–1280 (2010).
47. R. Atashkooei et al. "Runout tracking in electrical motors using self-mixing interferometry," *IEEE Trans. Mechatron.* **19**, 184–190 (2014).
48. M. Chen et al., "Damping microvibration measurement using laser diode self-mixing interference," *IEEE Photonics J.* **6**(3), 5500508 (2014).
49. S. Donati and G. Martini, "Speckle-pattern intensity and phase second-order conditional statistics," *J. Opt. Soc. Am.* **69**, 1690–1694 (1979).
50. V. Contreras, J. Lonnquist, and J. Toivonen, "Edge filter enhanced self-mixing interferometry," *Opt. Lett.* **40**, 2814–2017 (2015).
51. M. Norgia, D. Melchionni, and S. Donati, "Exploiting the FM-signal in a laser-diode SMI by means of a Mach-Zehnder filter," *IEEE Photonics Technol. Lett.* **29**, 1552–1555 (2017).
52. S. Donati and M. Norgia, "Self-mixing interferometer with a laser diode: unveiling the FM channel and its advantages respect to the AM channel," *IEEE J. Quantum Electron.* **53**(5), 1–10 (2017).
53. H. Matsumoto, "Alignment of length-measuring IR laser interferometer using laser feedback," *Appl. Opt.* **19**, 1–2 (1980).
54. S. Merlo and S. Donati, "Reconstruction of displacement waveforms with a single-channel laser-diode feedback interferometer," *IEEE J. Quantum Electron.* **33**, 527–531 (1995).
55. G. Plantier, C. Bes, and T. Bosch, "Behavioral model of a self-mix laser diode sensor," *IEEE J. Quantum Electron.* **41**, 1157–1167 (2005).
56. Y. Fan et al., "Improving the measurement performance for a self-mixing interferometry-based displacement sensing system," *Appl. Opt.* **50**, 5064–5072 (2011).
57. A. Magnani et al., "Self-mixing digital closed-loop vibrometer for high accuracy vibration measurements," *Opt. Commun.* **365**, 133–139 (2016).
58. D. Melchionni et al., "Development of a design tool for closed-loop digital vibrometer," *Appl. Opt.* **54**(32), 9637–9643 (2015).
59. F. Gouaux, N. Sarvagent, and T. Bosch, "Absolute distance measurement with an optical feedback interferometer," *Appl. Opt.* **37**, 6684–6689 (1998).
60. D. Guo, M. Wang, and H. Xiang, "Self-mixing interferometry based on a double-modulation technique for absolute distance measurement," *Appl. Opt.* **46**(9), 1486–1491 (2007).
61. K. Kou et al., "Injected current reshaping in distance measurement by laser self-mixing interferometry," *Appl. Opt.* **53**(27), 6280–6286 (2014).
62. J. Schoukens, R. Pintelon, and H. Van Hamme, "The interpolated fast Fourier transform: a comparative study," *IEEE Trans. Instrum. Meas.* **41**, 226–232 (1992).
63. M. Nikolić et al., "Approach to frequency estimation in self-mixing interferometry: multiple signal classification," *Appl. Opt.* **52**, 3345–3350 (2013).
64. M. Norgia, D. Melchionni, and A. Pesatori, "Self-mixing instrument for simultaneous distance and speed measurement," *Opt. Laser Eng.* **99**, 31–38 (2017).

Silvano Donati is an emeritus professor at the University of Pavia, Italy. He received his degree in physics from the University of Milano in 1966 and has been full professor at the University of Pavia from 1981 to 2010. He is the author of more than 300 journal papers and has written two books. His current research interests include SMI and photonic systems. He is a member of SPIE, life fellow of IEEE, and emeritus fellow of OSA.

Michele Norgia is a full professor at Politecnico di Milano, Italy. He graduated with honors in electrical engineering from the University of Pavia in 1996 and joined Politecnico di Milano in 2006. He has authored over 150 papers published in international journals or conference proceedings. His main research interests are optical and electronic measurements. He is senior member of IEEE.